Preparation of Highly Ordered Cubic Mesoporous WO 3 /TiO 2 Films and Their Photocatalytic Properties

ARTICLE *in* CHEMISTRY OF MATERIALS · FEBRUARY 2006

Impact Factor: 8.35 · DOI: 10.1021/cm0522782

2 AUTHORS:

Jia Hong Pan
National University of Singapore
43 PUBLICATIONS **1,313** CITATIONS

SEE PROFILE

Wan In Lee
Inha University
157 PUBLICATIONS **4,356** CITATIONS

SEE PROFILE

Preparation of Highly Ordered Cubic Mesoporous WO_3/TiO_2 Films and Their Photocatalytic Properties

Jia Hong Pan and Wan In Lee*

Department of Chemistry, Inha University, Incheon, 402-751 Korea

Received October 14, 2005. Revised Manuscript Received December 2, 2005

Highly ordered cubic mesoporous WO_3/TiO_2 thin films were prepared by spin coating via an evaporation-induced self-assembly (EISA) process, employing metal alkoxides as inorganic precursors and Pluronic F127 as a structure-directing agent. With the incorporation of WO_3 into TiO_2, the ordering of the mesopore structure has been appreciably improved. That is, the presence of 2−6 mol % WO_3 retards the crystallization to the anatase phase, and this leads to the relative stabilization of the mesopore structure. The characterization results suggest that the majority of incorporated W species are located at the surface of the mesopore wall instead of doping into the TiO_2 lattice. For the prepared cubic mesoporous WO_3/TiO_2 thin films, the photocatalytic activity in decomposing 2-propanol in the gas phase was optimized at 4 mol % of WO_3 concentration. Its photocatalytic activity was 2.2 times that of a mesoporous TiO_2 film and 6.1 times that of a nonporous TiO_2 film derived from a typical sol−gel method. The enhanced photocatalytic activity of WO_3/TiO_2 is ascribed to the increase in surface acidity.

Introduction

Recently, the fabrication of mesoporous TiO_2 has drawn considerable attention due to the variety of its potential applications such as photocatalysts,[1] electrochromic devices,[2] photovoltaics,[3] host−guest chemistry,[4] and luminescent devices.[5] The so-called evaporation-induced self-assembly (EISA) process, initiated by Brinker's group, has realized a facile fabrication of mesoporous TiO_2 in thin film form.[6−11] With solvent evaporation, the concentration of the surfactant in the sol solution begins to exceed the critical micelle concentration, and the self-assembly procedure is triggered at the same time.[12−14] The 2D-hexagonal or 3D-cubic mesophase of TiO_2 can be selectively controlled by a subtle adjustment of the initial sol composition as well as the aging condition during the EISA process.

One of the promising applications of these mesoporous TiO_2 films would be their use as photocatalysts in decomposing pollutants or in generating hydrogen by water splitting.[15,16] Despite their low crystallinity, the mesoporous TiO_2 structures can be an efficient photocatalyst due to their ultrahigh surface area and greatly organized pore structures. In most cases, mesoporous TiO_2 has been studied for the decomposition of pollutants in aqueous solution.[17−19] However, they would be more efficient in the treatment of gas-phase organic pollutants since the mass transfer of pollutant molecules into the mesopore of TiO_2 is regarded as a rate-determining step in the photocatalytic reaction and fast diffusion is expected for gas-phase reactants. It is also expected that the cubic mesoporous film would offer higher photocatalytic efficiency than the hexagonal one since the mesopore channels of cubic mesostructures are open on the surface of the film regardless of the mesophase orientation, whereas those of hexagonal mesophases are parallel to the substrate and are not open on the film surface.

* To whom correspondence should be addressed. Telephone: +82-32-863-1026. Fax: +82-32-867-5604. E-mail: wanin@inha.ac.kr.

(1) Yu, J. C.; Wang, X. C.; Fu, X. Z. *Chem. Mater.* **2004**, *16*, 1523.
(2) Choi, S. Y.; Mamak, M.; Coombs, N.; Chopra, N.; Ozin, G. A. *Nano Lett.* **2004**, *4*, 1231.
(3) Vogel, R.; Meredith, P.; Kartini, I.; Harvey, M.; Riches, J. D.; Bishop, A.; Heckenberg, N.; Trau, M.; Rubinsztein-Dunlop, H. *Chem. Phys. Chem.* **2003**, *4*, 595.
(4) Perez, M. D.; Otal, E.; Bilmes, S. A.; Soler-Illia, G. J. A. A.; Crepaldi, E. L.; Grosso, D.; Sanchez, C. *Langmuir* **2004**, *20*, 6879.
(5) Frindell, K. L.; Bartl, M. H.; Popitsch, A.; Stucky, G. D. *Angew. Chem., Int. Ed.* **2002**, *41*, 959.
(6) Brinker, C. J.; Lu, Y.; Sellinger, A.; Fan, H. *Adv. Mater.* **1999**, *11*, 579.
(7) Alberius, P. C. A.; Frindell, K. L.; Hayward, R. C.; Kramer, E. J.; Stucky, G. D.; Chmelka, B. F. *Chem. Mater.* **2002,** *14*, 3284.
(8) (a) Grosso, D.; Soler-Illia, G. J. A. A.; Crepaldi, E. L.; Cagnol, F.; Sinturel, C.; Bourgeois, A.; Brunet-Bruneau, A.; Amenitsch, H.; Albouy, P. A.; Sanchez, C. *Chem. Mater.* **2003**, *15*, 4562. (b) Crepaldi, E. L.; Soler-Illia, G. J. A. A.; Grosso, D.; Cagnol, F.; Ribot, F.; Sanchez, C. *J. Am. Chem. Soc.* **2003**, *125*, 9770. (c) Crepaldi, E. L.; Soler-Illia, G. J. A. A.; Grosso, D.; Sanchez, C. *New J. Chem.* **2003**, *27*, 9.
(9) Bosc, F.; Ayral, A.; Albouy, P. A.; Datas, L.; Guizard, C. *Chem. Mater.* **2004**, *16*, 2208.
(10) Tian, B.; Liu, X.; Tu, B.; Yu, C.; Fan, J.; Wang, L.; Xie, S.; Stucky, G. D.; Zhao, D. *Nature Mater.* **2003**, *2*, 159.
(11) Wang, X.; Yu, J. C.; Yip, H. Y.; Wu, L.; Wong, P. K.; Lai, S. Y. *Chem. Eur. J.* **2005**, *11*, 2997.
(12) Lu, Y.; Ganguli, R.; Drewien, C. A.; Anderson, M. T.; Brinker, C. J.; Gong, W.; Guo, Y.; Soyez, H.; Dunn, B.; Huang, M. H.; Zink, J. I. *Nature* **1997**, *389*, 364.
(13) Grosso, D.; Cagnol, F.; Soler-Illia, G. J. A. A.; Crepaldi, E. L.; Amenitsch, H.; Brunet-Bruneau, A.; Bourgeois, A.; Sanchez, C. *Adv. Funct. Mater.* **2004**, *14*, 309.
(14) Yu, C.; Tian B.; Zhao, D. *Curr. Opin. Solid State Mater. Sci.* **2003**, *7*, 191.
(15) Linsebiler, A. L.; Lu, G.; Yates, J. T. *Chem. Rev.* **1995**, *95*, 735.
(16) Fujishima, A.; Rao, T. N.; Tryk, D. A. *J. Photochem. Photobiol. C: Photochem. Rev.* **2000**, *1*, 1.
(17) Bosc, F.; Ayral, A.; Albouy, P.-A.; Guizard, C. *Chem. Mater.* **2003**, *15*, 2463.
(18) Zhao, L.; Yu, Y.; Song, L.; Hu, X.; Larbot, A. *Appl. Surf. Sci.* **2005**, *239*, 285.
(19) Reddy, E. P.; Sun, B.; Smirniotis, P. G. *J. Phys. Chem. B* **2004**, *108*, 17198.

10.1021/cm0522782 CCC: $33.50
Published on Web 01/07/2006

Previously, we modified the surface of TiO_2 nanoparticles (Degussa P25) with WO_3.[20,21] The TiO_2 nanoparticles covered with a monolayer of WO_3 were much less agglomerated and more stably suspended in aqueous solution. Furthermore, the photocatalytic activity in decomposing gaseous 2-propanol was greatly improved owing to the dramatic increase in surface acidity. Similar results have also been observed by several other research groups.[22−24] Thus, it is expected that the WO_3-incorporated TiO_2 (WO_3/TiO_2) in the form of a mesoporous structure can further enhance photocatalytic efficiency.

The preparation of TiO_2-based composite mesoporous materials is currently attracting attention.[25−29] For example, Bartl et al. thermally post-treated Cd^{2+}-doped TiO_2 films with sulfur or selenium vapor. Then the synthesized mesoporous CdS/TiO_2 and $CdSe/TiO_2$ thin films showed an enhanced sensitivity to visible light.[25,26] Grosso et al. synthesized several mesoporous TiO_2-based binary metal oxide thin films with high thermal stability such as $SrTiO_3$ and $Co_{0.15}Ti_{0.85}O_{1.85}$ dielectric materials.[27] Frindell et al. reported that the addition of Ce(III) improves the long-range ordering of mesoporous TiO_2 films.[29] Lu et al. reported WO_3/TiO_2 mesoporous films applicable to bio-photoelectrodes.[30] However, the prepared mesoporous film had a wormlike structure, and the precise analysis of the composite structure was not provided.

In this paper, we report a facile and reproducible method for the preparation of highly ordered transparent cubic mesoporous WO_3/TiO_2 thin films with various compositions of WO_3. In the previous report, we indicated that the mesophases of TiO_2 thin films were selectively controlled by the speed of spin coating during the EISA process.[31] The cubic mesoporous TiO_2 thin films were obtained by spin coating at a low rpm, while the 2-D hexagonal mesoporous films were prepared at a high spin-coating speed. In the present work, the structure of cubic mesoporous WO_3/TiO_2 films derived by this method was fully characterized by XRD, TEM, XPS, Raman and UV−visible spectroscopy, and surface acidity measurement. WO_3/TiO_2 thin films were then tested as photocatalysts in decomposing gas-phase organics, and the role of WO_3 in photocatalytic behavior was also discussed.

Experimental Section

Preparation of Cubic Mesoporous TiO_2 and WO_3/TiO_2 Films and Nonporous TiO_2 Film. Cubic mesoporous TiO_2 and WO_3/TiO_2 thin films were derived from the mixed metal alkoxides in stoichiometric ratio stabilized in an acidic ethanol solution containing triblock copolymer. The preparation method was based on our previous report on mesoporous TiO_2 thin films.[31] In a typical experiment, titanium tetraisopropoxide (TTIP, 97%, Aldrich) was dissolved and stabilized in ethanol solution acidified with aqueous HCl for 10 min at room temperature. Tungsten(V) pentaethoxide (95%, Gelest), stabilized by 2 equiv of 2,4-pentadione, was then added with vigorous stirring. After the solution was stirred for an additional 10 min, the resultant W−Ti sol was added to the Pluronic F127 (Aldrich) ethanol solution dropwise. The molar ratio of the final composition in the Ti−W sol was as follows: (Ti + W)/F127/HCl/H_2O/ethanol = 1:0.005:1.75:10:25. The transparent sol was aged under mild agitation for 3 h and then deposited on a precleaned Pyrex glass (2.5 × 2.5 cm^2) substrate by spin coating. The spin speed was raised to 600 rpm with an acceleration of 300 rpm/s, and it was then maintained for 5 s. The resulting films were aged for 3 days in a closed chamber, the relative humidity (RH) of which was maintained at 60% by a saturated $Mg(NO_3)_2$ aqueous solution. The removal of F127 used as a liquid-crystal template was carried out by heating at 400 °C for 4 h (ramping rate: 1 °C/min) in air. The thickness of each calcined film was controlled to 300−320 nm.

For the comparison, TiO_2 films without the pore structure were prepared by a typical sol−gel method. TTIP (0.020 mol) was dissolved in 10 mL of *n*-propanol, and 0.040 mol of 2,4-pentadione was then added dropwise while cooling. An additional 14 mL of *n*-propanol and 1 mL of 0.1 M nitric acid were then added and stirred for 4 h to prepare the 0.8 M Ti-sol solution. The prepared Ti-sol was deposited on a Pyrex substrate by spin coating at 2000 rpm for 20 s, and the coated film was subsequently baked at 150 °C. After three coating and baking cycles, the resultant film was calcined at 400 °C for 4 h to obtain a nonporous anatase TiO_2 film with a 300 nm thickness.

Characterization of Mesoporous WO_3/TiO_2 Thin Films. X-ray diffraction (XRD) patterns for the TiO_2 and WO_3/TiO_2 films were obtained by using a Rigaku Multiflex diffractometer with a monochromated high-intensity Cu Kα radiation. XRD scanning was performed under ambient conditions over the 2θ region 0.8−4° at the rate of 0.1°/min (20 kV, 10 mA) and 20−60° at 2°/min (30 kV, 20 mA), respectively.

For the observation of prepared mesoporous thin films by TEM (Hitachi S-4500 transmission electron microscope operated at 250 kV), the samples were peeled off from the substrate, and the collected flakes were gently dispersed in methanol. The suspension was then dropped on a holey amorphous carbon film deposited on a Ni grid (JEOL Ltd.).

The optical transmissions for the films were recorded by a UV−visible spectrophotometer (Perkin-Elmer Lambda 40) in the wavelength range of 200−800 nm. Raman spectra were recorded on a FT Raman spectrophotometer (Brucker, RFS-100/S) equipped with a room-temperature InGaAs diode detector. The 514.5 nm line from the Ar^+ laser beam was used as an exciting source. The output of the incident laser power was about 130 mW, and the resolution of the spectra was 2 cm^{-1}.

X-ray photoelectron spectroscopy (XPS) analyses of the mesoporous WO_3/TiO_2 thin films were carried out in an ultrahigh vacuum (UHV) chamber with a base pressure below 5 × 10^{-9} Torr at room temperature. Photoemission spectra were recorded by a Sigma Probe Instrument (Thermo VG, U.K.) equipped with a standard monochromatic Al Kα excitation source ($h\nu$ = 1486.6 eV). The pass

(20) Kwon, Y. T.; Song, K. Y.; Lee, W. I.; Choi, G. J.; Do, Y. R. *J. Catal.* **2000**, *191*, 192.
(21) Song, K. Y.; Park, M. K.; Kwon, Y. T.; Lee, H. W.; Chung W. J.; Lee, W. I. *Chem. Mater.* **2001**, *13*, 2349.
(22) Keller, V.; Bernhardt, P.; Garin, F. *J. Catal.* **2003**, *215*, 129.
(23) Rampaul, A.; Parkin, I. P.; O'Neill, S. A.; DeSouza, J.; Mills, A.; Elliott, N. *Polyhedron* **2003**, *22*, 35.
(24) Fu, X. Z.; Clark, L. A.; Yang, Q.; Anderson, M. A. *Environ. Sci. Technol.* **1996,** *30*, 647.
(25) Bartl, M. H.; Boettcher, S. W.; Frindell, K. L.; Stucky, G. D. *Acc. Chem. Res.* **2005,** *38*, 263.
(26) Bartl, M. H.; Puls, S. P.; Tang, J.; Lichtenegger, H. C.; Stucky, G. D. *Angew. Chem., Int. Ed.* **2004**, *43*, 3037.
(27) Grosso, D.; Boissière, C.; Smarsly, B.; Brezesinski, T.; Pinna, N.; Albouy, P. A.; Amenitsch, H.; Antonietti, M.; Sanchez, C. *Nat. Mater.* **2004**, *3*, 787.
(28) Zárate, D. O.; Boissière, C.; Grosso, D.; Albouy, P. A.; Amenitsch, H.; Amoros, P.; Sanchez, C. *New J. Chem.* **2005**, *29*, 141.
(29) Frindell, K. L.; Tang, J.; Harreld, J. H.; Stucky, G. D. *Chem. Mater.* **2004**, *16*, 3524.
(30) Lu, Y.; Yuan, M.; Liu, Y.; Tu, B.; Xu, C.; Liu, B.; Zhao, D.; Kong, J. *Langmuir* **2005**, *21*, 4071.
(31) Pan, J. H.; Lee, W. I. *New J. Chem.* **2005**, *29*, 841.

energy and step size of low-resolution XPS scan were performed at 50 and 10 eV, respectively. For the high-resolution XPS scan, the parameters above were adjusted to 20 and 0.1 eV. The binding energy (BE) scale was calibrated by measuring a C 1s peak at 284.5 eV from the surface contamination. The resultant XPS spectra were simulated by assuming the photoelectron peaks as Gaussian line shape.

For the measurement of surface acidity, each mesoporous film was prepared in a large area and was scraped to obtain a 0.1 g of sample. The 0.1 g mesoporous sample was suspended in doubly distilled benzene and then titrated with 0.03 N *n*-butylamine benzene solution, using methyl red as an indicator whose endpoint lies between pH 4.8 and 5.9.

Measurement of Photocatalytic Activity. Cubic mesoporous TiO_2 and WO_3/TiO_2 thin films were tested as photocatalysts for the decomposition of 2-propanol in the gas phase. The gas reactor system used for this photocatalytic reaction is described elsewhere.[32] A mesoporous film was located in the center of a gastight reactor with a net volume of 200 mL. With injection of 1.6 and 3.2 μL of liquid 2-propanol and water, respectively, their partial pressures in the reactor were adjusted to 2 and 16 Torr, respectively. The total pressure of the reactor was then controlled to 700 Torr by adding 682 Torr of oxygen gas. The gas mixtures in the reactor were magnetically convected during the irradiation. The mixture of UV and visible light, which was generated from a 300 W Xe lamp equipped with a water filter to cut off infrared, was used as the irradiation source. On the surface of the photocatalytic film, the overall light intensity was 1.0 W/cm^2. After irradiation for a certain period of time, 0.5 mL of gas sample in the reactor was automatically picked up and sent to a gas chromatograph (Young Lin M600D) by using an autosampling valve system (Valco Instruments Inc. A60). The evolved CO_2 and remnant 2-propanol were detected by a methanizer installed between the GC column outlet and the FID detector.

Results and Discussion

The long-range ordering of the mesopore structure for the WO_3/TiO_2 composite films was analyzed by small-angle XRD patterns, as indicated in Figure 1a. The fwhm's of the (200) peak for the pure TiO_2 and 2, 4, 6, and 8% WO_3/TiO_2 films are 0.184, 0.157, 0.148, 0.172, and 0.202°, respectively. The (200) peak of the 4% WO_3/TiO_2 mesoporous film is considerably more narrow, and its peak intensity is twice that of the pure TiO_2 film. This indicates that the ordering of the mesopore structures can be notably improved by the incorporation of WO_3. Also the (110) and (111) peaks, which were obscure in the pure mesoporous TiO_2 film, were clearly resolved for 2 and 4% WO_3/TiO_2 films. From the relative positions of these diffraction peaks, the prepared mesostructures were determined to be the $Im\bar{3}m$ 3D cubic phase.[1,5,7] A further increase in WO_3 over 4 mol % decreased the ordering of the mesopore array. Wide-angle XRD patterns obtained from several WO_3/TiO_2 films are shown in Figure 1b. Regardless of the WO_3 concentration, they were shown as pure anatase without impurity phases. However, the intensity of the (101) peak at 25.6° gradually decreased, and its peak width was broader with an increase in WO_3 compositions in the TiO_2 mesoporous film. Obviously, the incorporation of WO_3 hindered the crystallization of TiO_2 during the calcinations at 400 °C. In general, the mesopore structures are becoming distorted or collapsed while crystallizing at the calcination temperature, and this lowers the long-range ordering of the mesopores, as commonly observed in the formation of bulk mesoporous transition metal oxides. Thus, we suggest that the improvement of long-range ordering for the mesoporous WO_3/TiO_2 film is caused by the comparatively low crystallinity.

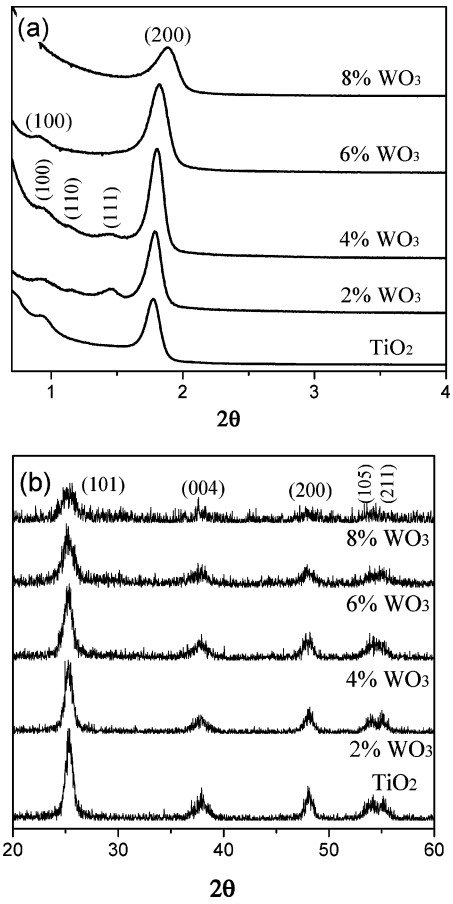

Figure 1. Small-angle (a) and wide-angle (b) XRD patterns for the mesoporous WO_3/TiO_2 thin films calcined at 400 °C.

TEM images for several mesoporous WO_3/TiO_2 films calcined at 400 °C are shown in Figure 2. The films containing 2, 4, and 6 mol % of WO_3 had highly ordered cubic mesoporous structures. The d(100) of the cubic mesopore was estimated at 10.0 nm, which corresponds to the result of 10.03 nm determined from the XRD patterns. On the other hand, the ordering of mesopores for the film containing 8 mol % of WO_3 was not so high. Its mesophase was regarded as a mixture of the cubic and wormlike structure. The overall trend of long-range ordering as a function of WO_3 concentration was consistent with the results of small-angle XRD.

Figure 3 shows the UV−visible spectra indicating the transparency of the mesoporous WO_3/TiO_2 films in a thickness of about 300 nm. All the mesoporous films showed higher transmittance than 80% over the entire visible light range, which would be caused by their high porosity and surface uniformity. However, the transmittance of the WO_3/TiO_2 films was gradually decreased with an increase in incorporated WO_3. The segregated amorphous WO_3 domains

(32) Chae, S. Y.; Park, M. K.; Lee, S. K.; Kim, T. Y.; Kim, S. K.; Lee, W. I. *Chem. Mater.* **2003**, *15*, 3326.

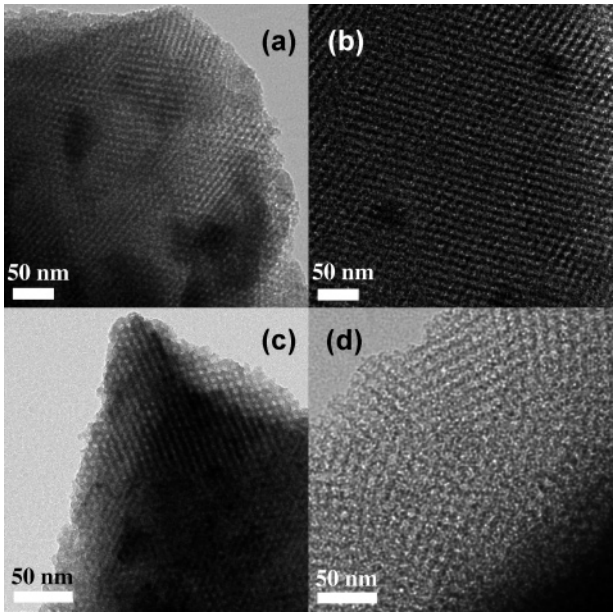

Figure 2. TEM images for several mesoporous WO_3/TiO_2 thin films calcined at 400 °C. The concentrations of WO_3 are 2 (a), 4 (b), 6 (c), and 8 (d) mol %.

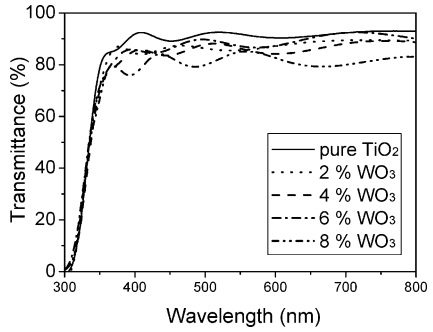

Figure 3. Transmittance spectra obtained by a UV−visible spectrophotometer for the cubic mesoporous TiO_2 and several WO_3/TiO_2 thin films calcined at 400 °C.

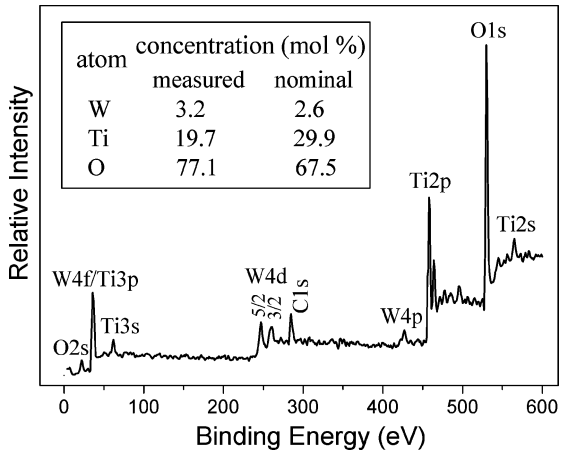

Figure 4. XPS survey spectrum of the mesoporous 8 mol % WO_3/TiO_2 thin films calcined at 400 °C.

on the surface of TiO_2 mesopores or in the grain boundaries could be responsible for this loss in transmittance.

XPS measurements were performed to elucidate the surface chemical composition and the oxidation state for the mesoporous WO_3/TiO_2 thin films. Figure 4 shows the XPS survey spectrum for the mesoporous 8 mol % WO_3/92 mol % TiO_2 film calcined at 400 °C. The XPS peaks indicate

Table 1. XPS Analysis Result for the Cubic Mesoporous TiO_2 and WO_3/TiO_2 Thin Films

peaks		TiO_2	4% WO_3	8% WO_3
Ti $2p_{3/2}$		458.50	458.44	458.37
Ti $2p_{1/2}$		464.28	464.00	463.89
Ti 3p			37.04	37.10
	(Ti−O)	529.96	529.89	529.81
O 1s	(−OH)	531.33	531.95	532.01
	(C−O)	532.78	533.01	533.06
	(H_2O)		534.26	534.30
W $4f_{7/2}$			35.22	35.27
W $4f_{5/2}$			37.42	37.47

that the WO_3/TiO_2 films contain Ti, W, O, and trace amounts of carbon, which originates from the residual carbon in the mesoporous film and the adventitious hydrocarbon in the XPS instrument itself. The determined concentration of W was 1.8 times higher than that of the nominal one, suggesting that relatively more W species are present on the surface of the mesoporous film (see inset of Figure 4). Figure 5 shows the high-resolution XPS spectra of Ti 2p, O 1s, and W 4f, which were taken on the surfaces of pure TiO_2 and 4 and 8% WO_3/TiO_2 mesoporous thin films, respectively. With the incorporation of W species, the intensity of Ti 2p was considerably decreased. This also suggests that relatively more W species are present on the surface of the mesopore structure. In addition, the binding energy of Ti 2p was slightly decreased as indicated in Figure 5a and Table 1. The slight decrease in binding energy suggests that some of Ti^{4+} is converted to a lower oxidation state, such as Ti^{3+}. As shown in Figure 5b, the O 1s band has been greatly modified with the introduction of the W species. For the pure mesoporous TiO_2, three oxygen contributions were taken into account. The peak at 529.96 eV was assigned to the oxygen bound to Ti, while the other peaks were related to the hydroxyl groups (BE = 531.33 eV) and the oxygen in C−O or C═O bonds (BE = 532.78 eV), respectively. On the other hand, the O 1s region of WO_3/TiO_2 was considerably broader and was fitted with four peaks. The peak at 529.8−529.9 eV contained contributions from both the Ti−O and W−O, which have similar binding energies. Besides the −OH and C−O peaks, an additional O 1s peak at around 534.26−534.30 eV appeared. This was assigned to the adsorbed H_2O on the surface of WO_3/TiO_2 mesoporous films. Also, the intensity of the −OH peak was considerably increased, compared to that of the pure mesoporous TiO_2 films. This clearly indicates that the mesoporous WO_3/TiO_2 composite thin films calcined at 400 °C have more hydroxyl groups as well as surface-adsorbed water. As shown in Figure 5c, the determination of the exact peak positions of W $4f_{7/2}$ and $4f_{5/2}$ was difficult because of the overlap with the Ti 3p peak. However, their positions are virtually the same as those of pure WO_3, suggesting that the oxidation state of the incorporated tungsten species is +6.

The Raman spectra of the mesoporous WO_3/TiO_2 thin films with different molar ratio calcined at 400 °C are shown in Figure 6. The bands at ca. 147, 196, 397, 516, and 639 cm^{-1} originate from the anatase phase of TiO_2. By introducing WO_3, an additional broad band appeared at ∼975 cm^{-1}. This was assigned to a terminal W═O stretching band which

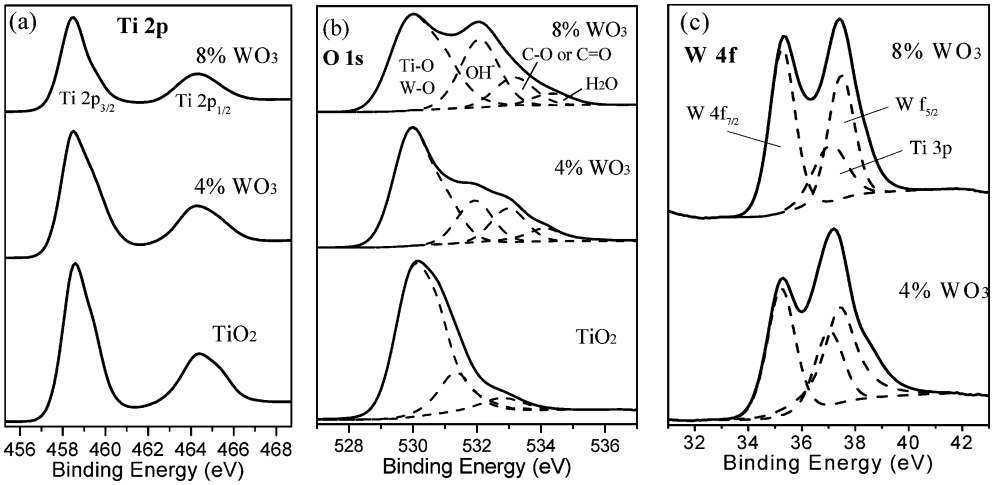

Figure 5. High-resolution XPS spectra and simulated Gaussian line shapes of Ti 2p (a), O 1s (b), and W 4f (c) region taken on the surface of pure TiO_2 and 4 and 8 mol % WO_3/TiO_2 mesoporous thin films.

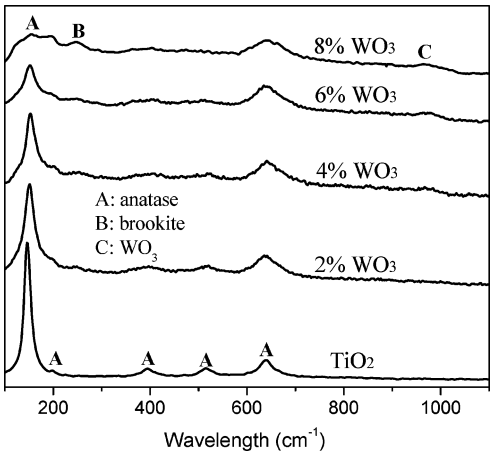

Figure 6. Raman spectra of several mesoporous WO_3/TiO_2 films calcined at 400 °C.

is common for all types of tungsten trioxide hydrates.[23,33,34] This supports the XPS result that adsorbed H_2O is contained in the WO_3/TiO_2 samples. However, the O−W−O stretching band at 805 ± 5 cm^{-1}, the main peak of crystallized monoclinic or orthorhombic WO_3, did not appear at all. This suggests that most of the incorporated WO_3 is highly dispersed over the TiO_2 mesoporous structure without forming large crystallized structures at 400 °C.

With an increase in incorporated WO_3, the bands from the anatase phase were gradually decreased in intensity and became broader. This is ascribed to the lower crystallinity of the anatase phase and is consistent with the results of the XRD patterns. In the Raman spectra, a weak peak at 246 cm^{-1}, considered to be originated from the brookite phase, which was not resolved by XRD, appeared. Its peak intensity increased with a corresponding increase in WO_3 concentration. Presumably, the incorporation of WO_3 in TiO_2 promotes the evolution of the brookite phase, while suppressing the formation of the anatase phase.

The photocatalytic activities of cubic mesoporous TiO_2 and WO_3/TiO_2 films of 300 nm thickness were evaluated. 2-Propanol was utilized as a model compound for the photocatalytic decomposition of a gas-phase pollutant. It was initially decomposed to acetone and then finally mineralized to CO_2 and H_2O. Thus, the photocatalytic activity was estimated in two ways. First, the decomposition of 2-propanol was monitored, as shown in Figure 7a. The photocatalytic decomposition was plotted as irradiation time vs ln[c], with the approximation of first-order kinetics.[20] That is, the photocatalytic reaction can simply be described by $-d[\mathbf{c}]/dt = k_r[\mathbf{c}]$, where [**c**] is the concentration of gaseous 2-propanol, t is the irradiation time, and k_r is the overall rate constant. Here, we defined the photocatalytic activity as k_r. Compared with the nonporous film derived from the spin coating of Ti-sol solution, the cubic mesoporous pure TiO_2 films presented 2.7 times greater photocatalytic activity in decomposing 2-propanol. The increase in photocatalytic activity despite the low crystallinity for the mesoporous structure would be due to the ultrahigh surface area of the mesoporous TiO_2. By the incorporation of WO_3 into the TiO_2 mesoporous structure, the photocatalytic activity was even more enhanced. The photocatalytic activity was maximized at 4 mol % of WO_3, and a further increase over 4% rapidly decreased its efficiency. The 4 mol % WO_3/TiO_2 cubic mesoporous film demonstrated 2.2 and 6.1 times greater photocatalytic efficiency than the pure cubic mesoporous TiO_2 film and the nonporous TiO_2 films, respectively. In evolving CO_2, a similar trend was observed, but the increment was relatively lower, as described in Figure 7b. It was found that the CO_2 evolved in 60 min of irradiation with 4 mol % mesoporous WO_3/TiO_2 films was 1.5 times greater than that with the pure mesoporous TiO_2 films. Likewise, it was 2.8 times greater than that with the nonporous TiO_2 films.

Figure 8 shows the acidity of mesoporous WO_3/TiO_2 as a function of the WO_3 composition. By the incorporation of WO_3, the surface acidity of the resultant mesoporous structures was considerably increased due to the highly acidic nature of WO_3. For the initial addition of WO_3, especially, the increment was very large. That is, by the introduction of 1 and 2 mol % WO_3, the surface acidity went up from 0.13 to 0.22 and 0.30 mmol/g, respectively. However, with a higher concentration of WO_3 over 6 mol %, the surface

(33) Santato, C.; Odziemkowski, M.; Ulmann, M.; Augustynski, J. *J. Am. Chem. Soc.* **2001**, *123*, 10639.
(34) Fernández-García, M.; Martínez-Arias, A.; Fuerte, A.; Cones, J. C. *J. Phys. Chem. B* **2005**, *109*, 6075.

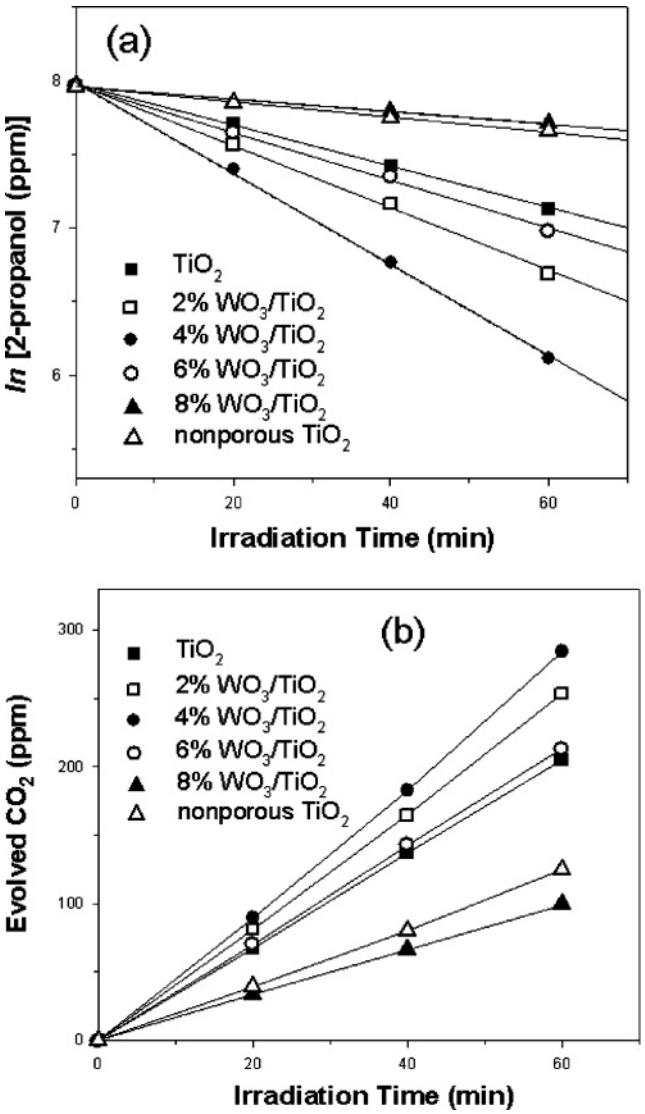

Figure 7. Photocatalytic decomposition rate of 2-propanol to acetone (a) and evolution rate of CO_2 (b) with several cubic mesoporous and nonporous films.

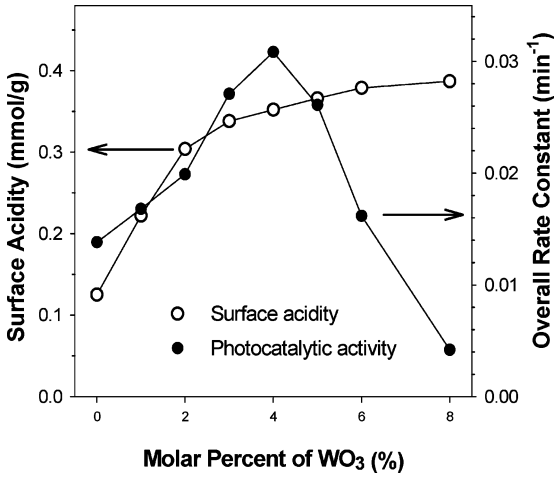

Figure 8. Surface acidity and photocatalytic activity of the mesoporous WO_3/TiO_2 thin films as a function of WO_3 concentration.

acidity was not appreciably changed. In Figure 8, the trend of photocatalytic activity as a function of WO_3 composition is also illustrated. The photocatalytic activity in decomposing 2-propanol was optimized in the range of 3−5 mol % of

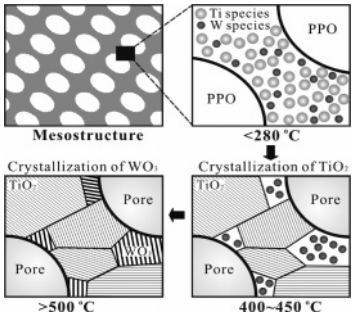

Figure 9. A scheme for the formation of the mesostructured WO_3/TiO_2 binary system during the heat treatment.

WO_3, where the surface acidity reached a plateau region. This result was similar to our previous reports on the surface modification of TiO_2 particles with WO_3.[20,21]

With the introduction of WO_3, the increase in surface area was not appreciable. The surface area of the cubic mesoporous TiO_2 film was 114 m^2/g, while that of the WO_3/TiO_2 films containing 2−8 mol % of WO_3 was 120−130 m^2/g. Thus, the enhancement of photocatalytic activity was not caused by the increase in surface area. As was reported previously, we believe that it is mainly due to the increase in surface acidity with the introduction of WO_3.[19−22] That is, as analyzed by the O 1s XPS spectra, the WO_3/TiO_2 thin films can adsorb a greater amount of organic molecules and OH^- or H_2O, which are necessary to initiate the photocatalytic reaction.

The crystallization of TiO_2 during the formation of the mesoporous structure by the EISA process has been delayed markedly compared to that of films derived by the typical sol−gel method. Several groups have reported that the mesoporous TiO_2 films calcined at 350 °C remained in the amorphous phase,[10,18,30] and that the phase transition to anatase was not complete even at 400 °C. By the addition of the W species, the crystallization of TiO_2 is further suppressed, as shown by the XRD data (Figure 1b). In general, a solid solution between TiO_2 and WO_3 can be formed with a heat-treatment temperature higher than 700 °C.[35,36] Even in this case, the level of WO_3 doping is lower than 1 mol %. Furthermore, it is well-known that the crystallization temperature of WO_3 is higher than that of TiO_2.[23] During the aging and drying steps in the EISA process, the Ti and incorporated W species are assumed to be mixed up uniformly, even though the complete mixing at the atomic level is not confirmed with the different reactivity and kinetics between the Ti and W precursors. With the subsequent heat treatment reaching up to 400 °C, TiO_2 itself will be crystallized first without forming a solid solution with WO_3. Thus, the remaining W species would be expelled to the grain boundary of the TiO_2 crystallites or to the surface of the mesopores, as suggested in Figure 9. Since the surface area of the mesopore is very large and the thickness of the wall is less than 7 nm, which is smaller than the typical grain size of TiO_2, the majority of WO_3 would be located on or near the surface of a mesopore. At a low concentration of

(35) Komornicki, S.; Radecka, M.; Sobaœ, P. *Mater. Res. Bull.* **2004**, *39*, 2007 and references therein.
(36) Li, X. Z.; Li, F. B.; Yang, C. L.; Ge, W. K. *J. Photochem. Photobiol. A: Chem.* **2001**, *141*, 209.

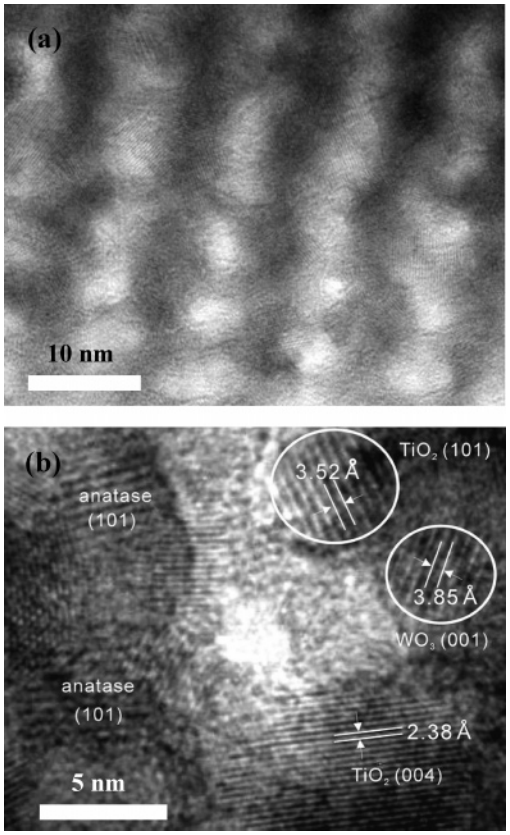

Figure 10. Representative HRTEM images for cubic mesoporous 6 mol % WO_3/TiO_2 thin films calcined at 400 °C (a) and 500 °C (b).

WO_3, it is expected that WO_3 preferentially binds to the surface of the TiO_2 grains with a high binding affinity between the TiO_2 and WO_3. Thus, most of the WO_3 exists in a form of highly dispersed molecular species on the surface of the TiO_2 mesopore. If the concentration of WO_3 is high, the extra WO_3 will be segregated by itself. This is clearly supported by the surface acidity result in which the surface acidity of WO_3/TiO_2 was dramatically increased with the initial addition of WO_3, whereas it was not appreciably increased at the higher concentrations of WO_3 over 4 mol %. In this circumstance, the state of WO_3 would be the mixtures of highly dispersed molecular species, clusters, and segregated domains with low crystallinity.

To monitor the definite morphology of the incorporated WO_3 in the mesostructure, the cubic mesoporous WO_3/TiO_2 thin films containing 6 mol % of WO_3 were examined by high-resolution TEM. As shown in Figure 10a, the crystallinity of the cubic mesoporous film calcined at 400 °C was not high enough for a structural analysis. For the observation of the crystallized structure of WO_3, the same mesoporous sample was heat-treated at 500 °C, but the identification of the WO_3 phase by TEM was still very difficult since the WO_3 is not sufficiently crystallized at this temperature and is presumably well-dispersed as small clusters along the surface or grain boundaries of TiO_2. After several trials done and errors incurred, a crystallized WO_3 grain was monitored in a certain area around a mesopore, as indicated in Figure 10b. The fringe spacing of 3.85 Å was indexed to the (001) plane of the orthorhombic WO_3 phase.

Conclusions

In this work, we have synthesized transparent and highly ordered cubic mesoporous WO_3/TiO_2 thin films by the EISA process. We found that the introduction of 2−6 mol % WO_3 in TiO_2 mesoporous structures hinders the crystallization of the anatase phase, but the long-range ordering of the mesostructure was appreciably more organized. The characterization data for the films annealed at 400 °C indicate that the incorporated W species exist as WO_3 and that the majority of the WO_3 are located around the surface of mesopores instead of doping into TiO_2 lattice. This is because WO_3 and TiO_2 do not form a solid solution at this temperature and the crystallization temperature of WO_3 is relatively higher than that of TiO_2. By the incorporation of WO_3 the photocatalytic activity in decomposing gaseous 2-propanol was enhanced, and it was maximized at 4 mol % of WO_3. The enhanced photocatalytic activity of WO_3/TiO_2 was ascribed to the increased surface acidity which was induced by the WO_3 present on the surface of the mesopores.

Acknowledgment. The authors gratefully acknowledge the financial support of the Korean Science and Engineering Foundation (KOSEF R01-2003-000-10667-0) and the support project of the University ITRC Program.

CM0522782